Korean J. Chem. Eng., **26**(5), 1213-1219 (2009)
DOI: 10.1007/s11814-009-0214-7

Computational fluid dynamic simulation of MVG tray hydraulics

Taleb Zarei, Rahbar Rahimi†, and Mortaza Zivdar

Department of Chemical Engineering, University of Sistan and Baluchestan, Zahedan P.O. Box 98164-161, Iran
(*Received 26 December 2008 • accepted 1 March 2009*)

Abstract−The flow pattern and hydraulics of a Mini V-Grid valve (MVG) tray is predicted by using computational fluid dynamics simulation. A 3-D CFD model in the Eulerian framework was used. The simulation results for MVG tray are compared with that of sieve tray. The sieve tray geometry and operating conditions are based on the Solari and Bell's sieve tray [1]. The MVG tray differs from that of Solari and Bell's sieve tray solely by the difference in design of available openings for the flow of gas. The simulation results show that the clear liquid height and the pressure drop of MVG tray are lower than that of sieve tray whereas the liquid velocity is higher and contacts of phases are good. The simulation results of sieve tray are in agreement with the experimental data of Solari and Bell [1].

Key words: MVG Tray, Sieve Tray, Distillation, Two Phase Flow, CFD

INTRODUCTION

Distillation is a separation process of major importance in the chemical industries, and known as an energy-intensive process. Investigations and modeling work aimed at improving the performance of various distillation columns have been carried out by many researchers for many years [2-4].

Even though distillation is the first choice for separation of liquid mixtures, the low separation efficiency requires attempts to improve tray design and introduction of new trays. One of the major factors that favor distillation is the fact that large-diameter columns can be designed and built with confidence.

Many cross flow trays are simple sieve trays, i.e., decks which have many circular holes. Some trays have valves which can be vertically movable associated with the tray opening, and others have fixed deflectors. In the stationary valve tray, each tray opening includes a trapezoidal aperture in the plane of the tray deck, and a stationary deflector which overlies and is aligned with the aperture. The deflector and the adjacent deck surface define lateral outlet slots oriented to direct vapor which passes up through the aperture in directions generally transverse to the flow direction of liquid on the tray deck (Fig. 1). These trays are aimed to increase the tray load flexibility and to reduce tray back mixing and hence increase tray efficiency.

Most of the information on large size tray design is given in the form of empirical correlations obtained from a pilot plant, which does not take account of the actual flow patterns on the tray [1].

In recent years, there has been considerable academic and industrial interest in the use of computational fluid dynamics (CFD) to model the trays [5-14] that has proven to be a reliable method to overcome the shortages.

The key to proper CFD model is the estimation of the momentum exchange, or drag coefficient between the gas and liquid phases [15]. Krishna et al. [9] and Van Baten and Krishna [10] eliminated the need for the bubble diameter in the computation of the drag force between the bubbles and the liquid phase. Gesit et al. [11] developed a CFD model to simulate hydrodynamics, and Rahimi et al. [12] further developed the CFD model to predict temperature and concentration distributions of both liquid and vapor phases and determined the point and tray efficiencies of sieve tray. On the other

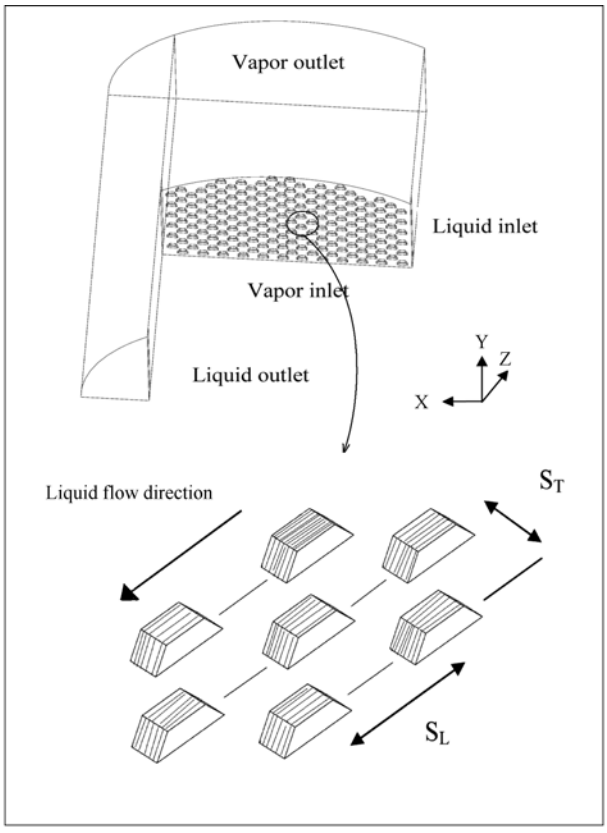

Fig. 1. Flow geometry and boundary conditions of MVG tray and a part of tray deck which shows stationary valve arrangements.

†To whom correspondence should be addressed.
E-mail: rahimi@hamoon.usb.ac.ir

hand, Wang et al. [14] used a 3-D pseudo-single-phase CFD model for liquid-phase velocity and concentration distribution on a distillation column tray. The column (overall) efficiency of a 10-tray column was estimated.

Their model does not predict point efficiency and vapor phase concentration distribution, and assumes a constant value for vapor (and liquid) volume fractions. Rahimi et al. [12,13] studied mass transfer efficiency of sieve trays by means of a 3-D two fluid CFD simulation.

Therefore, CFD has been established as a predictive and reliable tool that can be used to study different tray deck design and contacting mechanisms. An important advantage of CFD techniques is that geometry and scale effects are properly encapsulated [16].

Most of the previous reported CFD simulations in the open literature for the trays concerned the sieve tray, not other types of trays. Therefore, simulation of the hydrodynamics of Mini-V-Grid valve tray or MVG tray by using CFD has been attempted.

In recent years MVG trays have been installed successfully. The simulation of these valve trays is useful for understanding about flow pattern and hydraulics at different operating conditions. In this work a comparison between sieve tray and MVG tray based on a geometrical similarity by using CFD simulation has been done.

MODEL EQUATIONS

The dispersed gas and the continuous liquid phases at steady state condition are modeled in the Eulerian framework as two interpenetrating phases, having separate transport equations. The model equations are given in Table 1. The two-fluid conservation equations for adiabatic two-phase flow are presented as Eqs. (1) to (4).

The gas and the liquid volume fractions, r_G and r_L, are related by the summation constraint in Eq. (5).

The term M_{GL} in the momentum equations, Eqs. (3) and (4), represents interphase momentum transfer between the two phases.

Table 1. Model equations

$$\nabla\cdot(r_G\rho_G V_G)=0 \quad (1)$$

$$\nabla\cdot(r_L\rho_L V_L)=0 \quad (2)$$

$$0=-r_L\nabla P_L+r_L\rho_L g+\nabla\cdot(r_L\mu_{eff,L}(\nabla V_L+(\nabla V_L)^T))+M_{GL} \quad (3)$$

$$0=-r_G\nabla P_G+r_G\rho_G g+\nabla\cdot(r_G\mu_{eff,G}(\nabla V_G+(\nabla V_G)^T))-M_{GL} \quad (4)$$

$$r_G+r_L=1 \quad (5)$$

$$P_G=P_L \quad (6)$$

$$M_{GL}=\frac{3}{4}\frac{C_D}{d_G}r_G\rho_L|V_G-V_L|(V_G-V_L) \quad (7)$$

$$C_D=\frac{4}{3}\frac{\rho_L-\rho_G}{\rho_L}g d_G\frac{1}{V_{slip}} \quad (8)$$

$$V_{slip}=\frac{V_S}{r_G^{average}} \quad (9)$$

$$r_G^{average}=1-\exp\left[-12.55\left(V_S\sqrt{\frac{\rho_G}{\rho_L-\rho_G}}\right)^{0.91}\right] \quad (10)$$

$$M_{GL}=\frac{(r_G^{average})^2}{(1-r_G^{average})V_S^2}g(\rho_L-\rho_G)r_G r_L|V_G-V_L|(V_G-V_L) \quad (11)$$

$$U_{L,in}=1.5\frac{Q_L}{A_{cL}}\left[1-\left(\frac{2z}{L_w}\right)^2\right] \quad (12)$$

This is in final form, given by Eq. (11). It is assumed that the two phases share the same pressure field (Eq. (6)).

The closure models are required for interphase transfer quantities and turbulent viscosities. The situation on the tray becomes quite complex in the case of two way coupling (when volume fraction of dispersed phase is noticeable) between continuous phase and dispersed phase, since the presence of dispersed phase can affect turbulence in the continuous phase [15]. Hence, the standard k-ε turbulence model with the default model coefficients is used for simulating turbulence behavior of the liquid phase. The k-ε model is well treated in literature [15,17]. Turbulence models have not been used for the gas phase. The default values of model parameters are used: C_μ=0.09, C_1=1.44, C_2=1.92, σ_k=1, σ_ε=1.314

A CFX 10.0 software package on a 3.01 GHz CPU and 1.00 GB RAM, PC was used to solve the equations for the two fluid mixtures.

1. Closure Models

The interphase momentum transfer term, M_{GL}, is basically interphase drag force per unit volume. With the gas as the dispersed phase, the equation for M_{GL} is given by Eq. (6).

C_D is drag coefficient. Its value for the case of distillation is not well known. However, Fisher and Quarini [6] assumed a constant value of 0.44. This value is appropriate for large bubbles of spherical cap shape. However, for the froth flow regime, which is the dominant region in distillation, it is not applicable. Further, the bubbles are 10 to 20 mm in diameter with the bubble rise velocity of 1.5 m/s, and 2 to 5 mm in diameter, with the rise velocity of about 0.25 m/s [18]. Therefore, any equation for interphase transfer momentum that is independent of bubble diameter is appropriate.

Krishna et al. [9] have introduced a relation which is most suitable for CFD use. Their relation has been derived as Eq. (11), after substitution of Eqs. (8), (9) and (10) in Eq. (7). This is independent of bubble diameter.

In the drag coefficient relation, Eq. (8), V_{slip} is estimated from gas superficial velocity, V_S, and the average gas holdup fraction in the froth region, r_G^{ave}, by Eq. (9).

The average gas volume fraction relation, Eq. (10), is the Bennett et al [19] correlation.

TRAY GEOMETRY

Fig. 1 shows the geometry and boundary conditions of the simulated MVG tray. The characteristic of the simulated tray are shown in Table 2. Due to the existence of a symmetry plane for the purpose of reduction of computational effort, only half of the tray was simulated. Plane z=0 is the plane of symmetry.

The number of stationary valves for an MVG tray and the number of holes for sieve tray are 171 and 182, respectively. These ac-

Table 2. Tray specification

Column diameter	1.213 m
Weir length	0.925 m
Weir height	0.05 m
Down comer area	13%
Down comer clearance	0.038 m
Tray spacing	0.61 m

count for 7% of bubbling area for MVG tray and 5% for sieve tray. Only the gas entrances of the sieve and MVG tray differ from each other.

Fig. 1 shows that tray openings are positioned in adjacent longitudinal rows, and the apertures are positioned staggered from row-to-row. Hence an aperture in one row has a longitudinal position which is midway between the longitudinal positions of two longitudinally adjacent apertures in an adjacent row. Centers of the apertures that are distanced apart longitudinally in direction of the flow, S_L, are equal to 6.35 cm. The spacing between the centerlines of rows, S_T, is equal to 3.81 cm [20].

1. Wall and Boundary Conditions

The three recognizable gas-liquid mixture patterns from the inlet to the outlet of the downcomer are froth and aerated liquid mixture and clear liquid, respectively [21]. If jet contraction is eliminated, it can be assumed that the liquid is un-aerated as it leaves the downcomer.

Hence, there is a transition from essentially single phase (at the tray inlet) to two phase flow (on the tray deck) and both these factors make analysis in the region of the liquid entry quite difficult [22]. However, it is reasonable to assume a single liquid phase at near to the downcomer clearance as the holes are not made very close to the downcomer to avoid bubbles entering the downcomer.

In this study at the available operating condition, the Reynolds number criteria of the clear liquid inlet velocity are located in laminar flow. Thus, a parabolic velocity profile is applied to liquid inlet profile (Eq. (12)).

The liquid volume fraction at the liquid inlet and the liquid outlet were taken to be unity as only liquid enters through the downcomer clearance and only gas was assumed to exit through the vapor outlet and enter to the vapor inlet. So the outlet specification will be in agreement with the specification of inlet where only one fluid was assumed to enter.

A no-slip wall boundary condition was specified for the liquid phase and a free slip wall boundary condition was used for the gas phase. At the plane of symmetry, the normal component of velocity is zero and the gradient of the other variable in the transverse direction is taken to be zero.

A good initialization guess can reduce computational time and avoid divergence. The gas and liquid that were simulated are air and water at 25 degrees Celsius and at atmospheric pressure. Initially, the volume fraction of air and water in the whole of tray was specified. The volume fraction of water in clear liquid height is set 0.8, which is about average liquid volume fraction in the froth region. Above the clear liquid height gas volume fraction is 0.99. The downcomer assumed filled with water to the height of 0.275 m. The superficial gas velocity was used as an initial guess for the vertical component of the gas velocity throughout the computational domain and a uniform horizontal velocity distribution is equal to the liquid inlet velocity was specified for the froth region.

MESH GENERATION

The number of meshes has a significant role in the convergence and accuracy of the results. Grid convergence requires that after a certain grid size the numerical results do not change significantly as grid size is further decreased. Unstructured meshes have been used in these simulations because of the complexity of the MVG tray geometry. Unlike structured grids, coordinate transformation is not performed, and as a result they can be used for irregular geometries but at the expense of more complex computer programming. In the unstructured meshes, it is possible to get results for the actual number of holes and actual number of stationary valves in the MVG tray. Adjacent to the wall and adjacent to the vapor inlet finer meshes are used. Away from the tray deck the mesh sizes become larger. The type and number of meshes are shown in Table 3.

VELOCITY DISTRIBUTION

The used gas flow rates at a constant liquid flow rate of 0.0178

Table 3. Mesh configuration

Type of mesh	Number
Tetrahedral	366972
Pyramids	1188
Wedges	29333
Number of Nodes	86307
Number of elements	397493

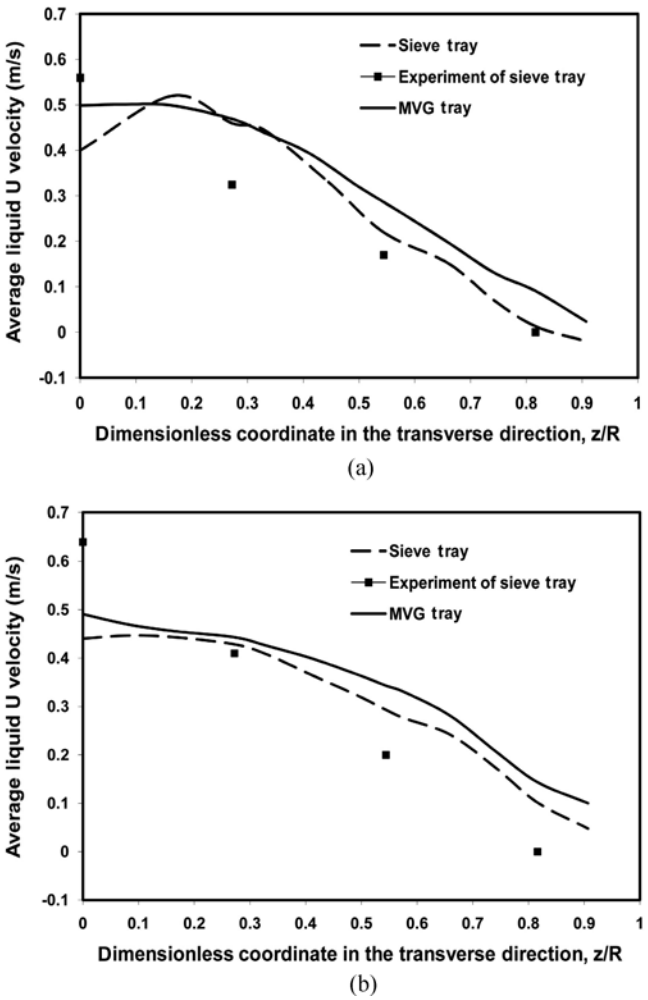

Fig. 2. Liquid velocity profile, $Q_L=17.8\times10^{-3}$ m^3/s, $F_S=0.462$ m/s $(kg/m^3)^{0.5}$: (a) upstream profile; (b) downstream profile.

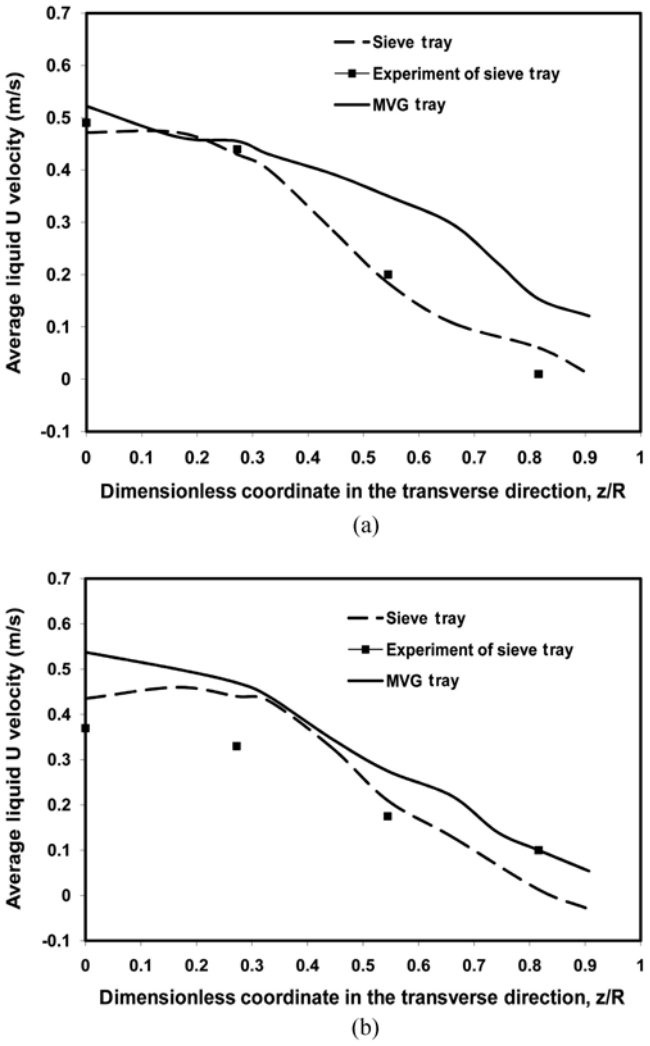

Fig. 3. Liquid velocity profile, Q_L=17.8×10^{-3} m^3/s, F_S=0.801 m/s (kg/m^3)$^{0.5}$: (a) upstream profile; (b) downstream profile.

m^3/s were gas flow rates with F_s factors equal to 0.462, 0.801, 1.015 and 1.464 m/s (kg/m^3)$^{1/2}$. The experimental data of Solari and Bell [1] for sieve tray are for F_S equal to 0.462 and 0.801 m/s (kg/m^3)$^{1/2}$. In Figs. 2 and 3, liquid horizontal velocities that have been predicted by the CFD simulations for the sieve and the MVG tray are shown with F_S=0.462 and 0.801. Experimental data of Solari and Bell [1] are also included for the purpose of validating the simulation results of sieve tray. The authors estimated the average velocity of the fluid by dividing the distance between two consecutive probes located in the same longitudinal row by the difference in mean residence time between two probes. The probes are held about 0.038 m above tray floor. Referring to Fig. 4, velocities were determined between the probe line composed of probes 5, 6, 7, 8 and probe line 9, 10, 11, 12, respectively. Velocities were also measured between this last probe and the line 13, 14, 15, 16, respectively. The first calculation yields an average velocity distribution in the middle section of the tray (upstream profile). The second approximates the velocity distribution at the tray outlet (downstream profile) [1].

To compare the experimental measurements with the CFD predictions, line integrals of the horizontal component of the liquid velocity were taken on the plane y=0.038 m between x=0.209 m and x=0.438 m. The resulting velocity profiles have been referred to as the upstream profiles. Similarly, line integrals were taken between x=0.438 m and x=0.667 m as the downstream profiles.

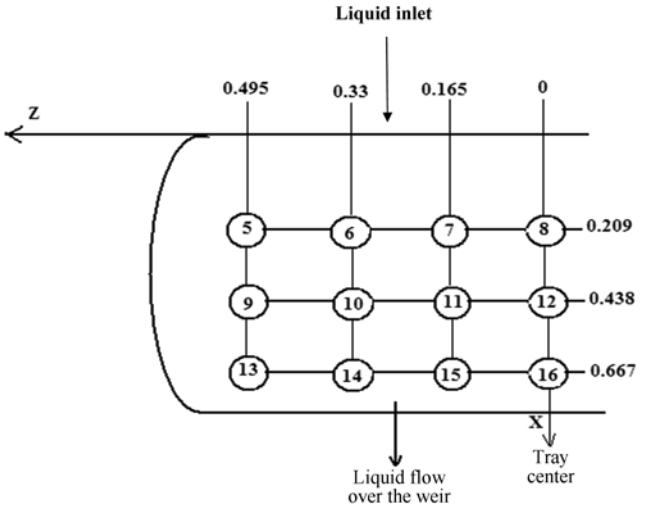

Fig. 4. Experimental probe layout of solari and Bell [1].

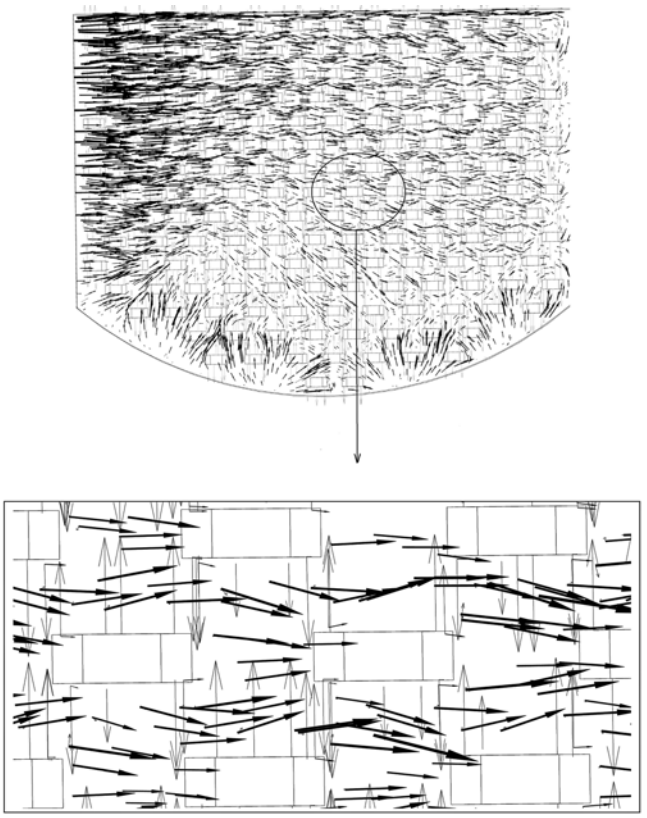

Fig. 5. Liquid (Bold vectors) and gas (thin vectors) velocity vectors at 5 mm above the tray deck, Q_L=17.8×10^{-3} m^3/s, F_S= 0.462 m/s (kg/m^3)$^{0.5}$.

The CFD simulation results have a good agreement with the experimental data of Solari and Bell [1]. Figs. 2 and 3 show that the liquid velocity value in the MVG tray is higher than that of the sieve tray. This is more obvious close to the wall at the given gas flow

rates. The deduction of less existence of stagnation points is advantageous when effects such as fouling and polymerization are a concern.

A non-uniform liquid velocity distribution is observed in all cases. The liquid velocity decreases by moving from the tray center toward the tray wall. The influence of gas rate on the liquid-velocity distribution is obvious by considering that in the Figs. 2 and 3 F_s are 0.462 and 0.801 m/s $(kg/m^3)^{1/2}$, respectively.

The gas and the liquid velocity vectors are given in Fig. 5. The path of gas is tangential to the tray deck (thin vectors) and perpendicular to the liquid path (Bold vectors). The horizontal paths of gas on the tray deck reduce the liquid entrainment for MVG tray and set a good contact between the two phases. The velocity distribution in the MVG tray is higher than that of the sieve tray, or retention time in the MVG tray is lower than the sieve tray. But a more intense contacting can compensate for lower retention time and a higher liquid velocity increases the capacity of the MVG tray.

CLEAR LIQUID HEIGHT, FROTH HEIGHT, LIQUID HOLDUP AND PRESSURE DROP

Clear liquid height is defined as the height of liquid that would exist on the tray in the absence of vapor flow. Using this definition, the clear liquid height has been calculated as the tray spacing multiplied by the volume average of the liquid volume fraction above the bubbling area of the tray floor [11].

The froth region is usually defined as the region in which the liquid volume fraction is greater than 10%. The average froth height has been calculated as the area average (over the tray deck (X, Z) plane) of the vertical distance (y) from the tray floor at which the liquid volume fraction starts to fall bellow 10%. Liquid hold up fraction in froth is often defined as the ratio of clear liquid height to froth height. Figs. 6 and 7 show these variables versus F_s.

Fig. 6(a) shows the clear liquid height against F_S for both sieve and MVG trays. The increasing of the F_S at a constant liquid flow rate has caused a decrease of the clear liquid height for both trays. The clear liquid height for MVG tray is less than sieve tray in all operating conditions.

Increase of the gas flow rate leads to the increase of froth height. Fig. 6(b) shows that froth height in the MVG is higher than Sieve tray.

Fig. 7(b) shows that the pressure drop in the tray has been decreased by increasing the gas flow rate, and the pressure drop in

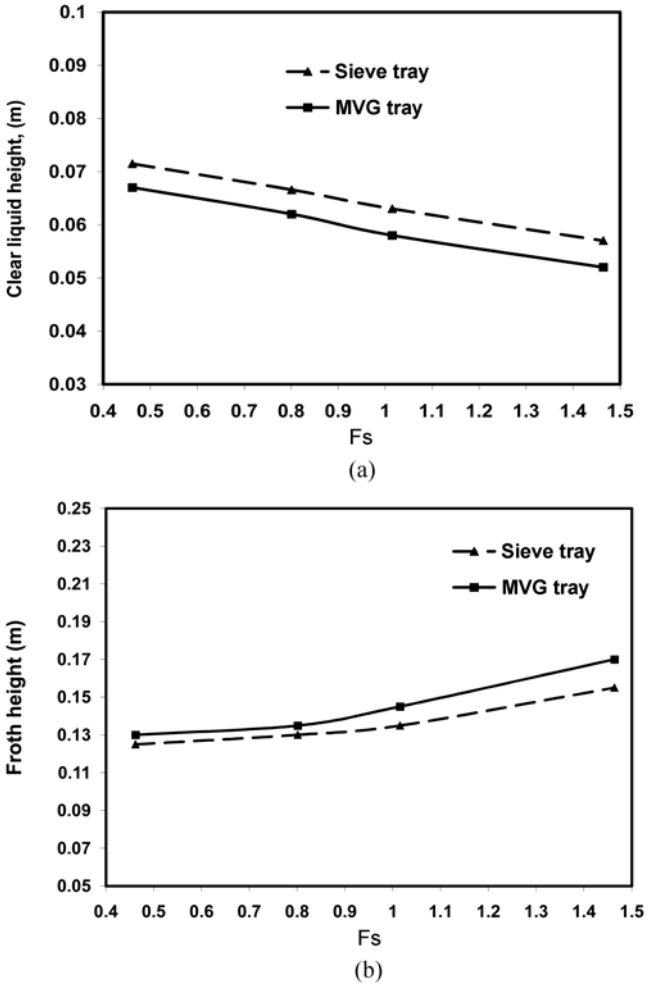

Fig. 6. (a) Clear liquid height as a function of F-factor (b) froth height as a function of F-factor.

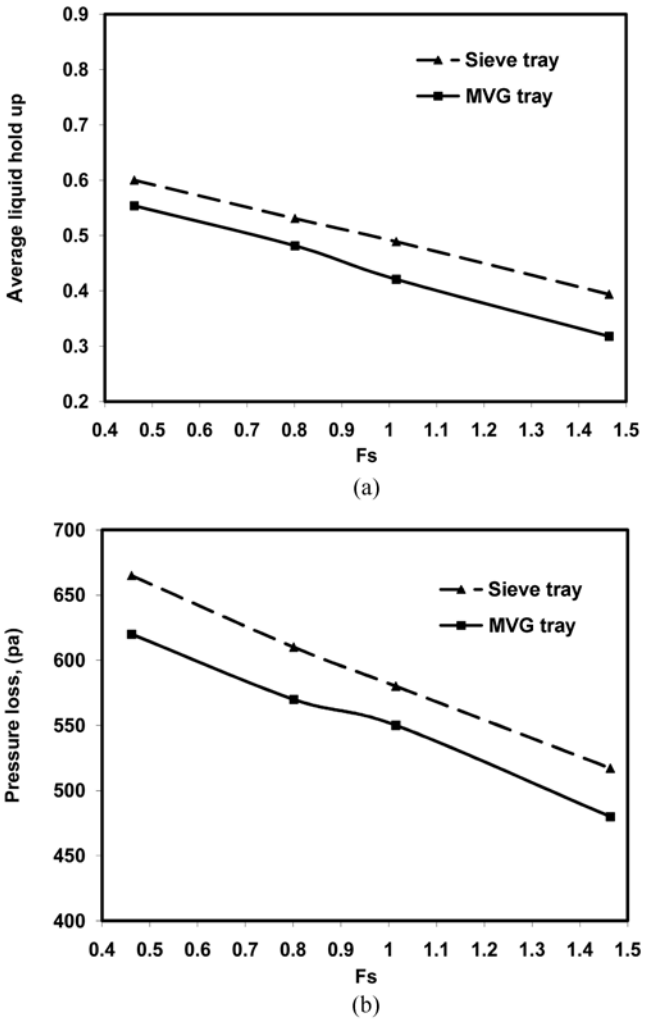

Fig. 7. (a) Average liquid hold up as a function of F-factor (b) pressure loss as a function of F-factor.

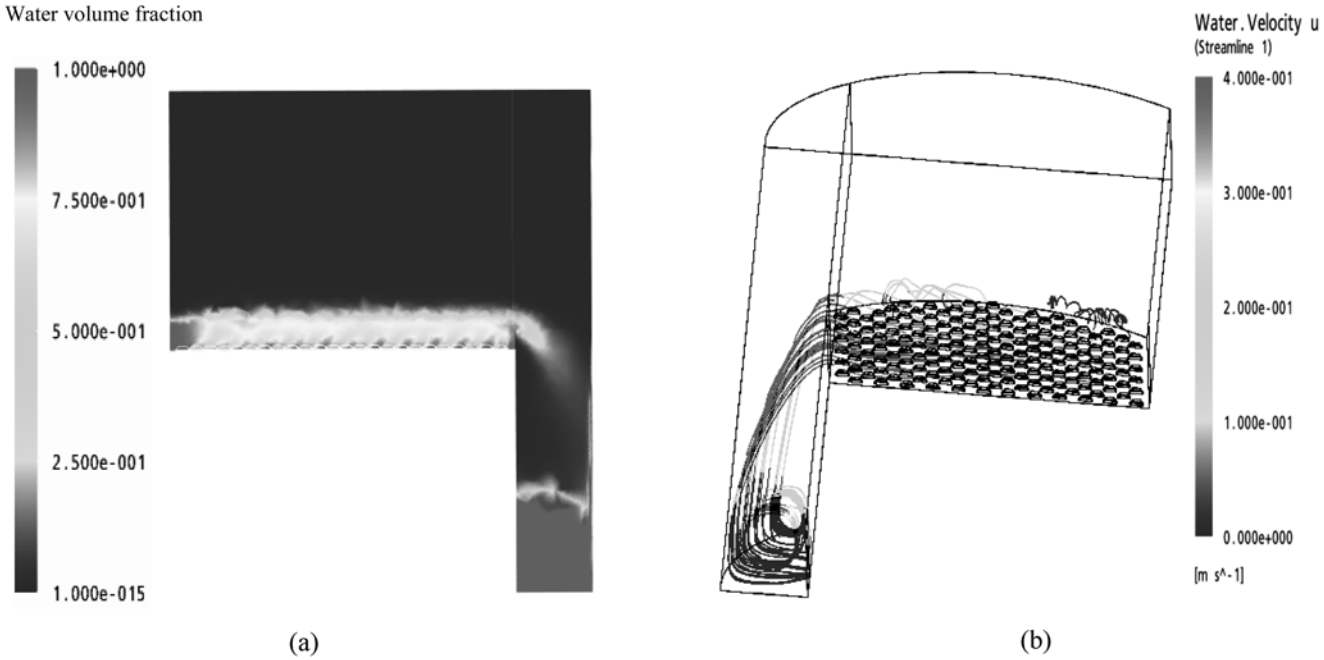

Fig. 8. (a) Liquid volume fraction profiles at the plane (x-y) and Z=0.2 m, (b) Stream line profiles of water velocity at the plane (x-z) and Y=0.038 m, F_S=0.462 m/s (kg/m^3)$^{0.5}$, Q_L=17.8×10^{-3} m^3/s.

the MVG is less than that of the sieve tray. Because of vacuum formation at the trapezoidal opening of each valve, the pressure drop at stationary valves is less than for sieve tray, despite physical obstruction to the flow of gas.

Fig. 8(a) shows liquid volume fraction contour for the MVG tray at the plane (X-Y) and at Z=0.2 m with F_S=0.462.

Fig. 8(b) shows water velocity streamline at F_S=0.462 from liquid inlet to the down comer liquid outlet. As gas separation also occurs in the downcomer, simulation of the tray should consider the downcomer effects.

CONCLUSION

Attempts have been made to predict the flow pattern and hydraulics of commercial-scale stationary valve trays. The results were compared with that of sieve tray by means of computational fluid dynamics. The comparison was based on the geometrical similarity of trays and near equality of the opening area. The direction of gas outlet from the openings is perpendicular to the sieve tray deck and tangential to the tray deck for the MVG tray. The velocity distribution, clear liquid height, froth height, liquid hold up and pressure drop was calculated. It was found that the pressure drop and the clear liquid height of the MVG tray is less than that of sieve tray at the same operating conditions. Good contacting between the two phases, lower pressure drop and clear liquid height, higher liquid velocity and froth height is observed in the simulation of MVG tray than sieve tray. These characteristics indicate a higher capacity of MVG tray than those of sieve tray. Experimental data are scarce, so extensive research efforts should be dedicated to provide experimental data suitable for validation of more complex trays than sieve or stationary valve trays. Similarity criteria should be redefined for the purpose of scale up.

NOMENCLATURE

A_{CL} : liquid clearance area [m^2]
CD : drag coefficient [-]
d_G : mean bubble diameter [m]
F_S : F factor=$V_S\sqrt{\rho_G}$ [m/s (kg/m^3)$^{0.5}$]
g : gravity acceleration [m/s^2]
L_w : inlet weir length [m]
M_{GL} : lnterphase momentum transfer [kg·m^{-2}·S^{-2}]
Np : number of phases
P_G : gas phase pressure [N m^{-2}]
P_L : liquid phase pressure [N m^{-2}]
Q_L : liquid volumetric flow rate [m^3/s]
r_G^{ave} : average gas holdup fraction in froth [-]
r_L : liquid-phase volume fraction [-]
r_G : gas-phase volume fraction [-]
$U_{L,in}$: x-component of liquid velocity at the inlet and the outlet boundary conditions [m/s]
V_G : gas phase velocity vector [m/s]
V_L : liquid phase velocity vector [m/s]
V_S : gas phase superficial velocity based on the bubbling area [m/s]
V_{slip} : slip velocity [m/s]
x : coordinate position in the direction of liquid flow across tray [m]
y : coordinate position in the direction of vapor flow across tray [m]
z : coordinate position in the transverse direction to liquid flow across tray [m]
$\mu_{eff,L}$: effective viscosity of liquid [kg·m^{-1}·s^{-1}]
$\mu_{eff,G}$: effective viscosity of gas [kg·m^{-1}·s^{-1}]
ρ_G : gas density [kg/m^3]

ρ_L : liquid density [kg/m^3]
k : turbulent kinetic energy [J kg^{-1}]
ε : dissipation rate of k [w kg^{-1}]
σ_k, σ_ε : turbulent Prandtl numbers for k-ε
C_1, C_2, C_μ : constants of the k-ε model

REFERENCES

1. B. Solari and R. L. Bell, *AIChE J.*, **32**, 640 (1986).
2. Q. S. Li, C. Ying Song, H. L. Wu, H. Liu and Y. Q. Qian, *Korean J. Chem. Eng.*, **25**, 1509 (2008).
3. S. Pradhan and A. Kannan, *Korean J. Chem. Eng.*, **22**, 441 (2005).
4. X. H. Wang, Y. D. Hu and Y. G. Li, *Korean J. Chem. Eng.*, **25**, 402 (2008).
5. B. Mehta, K. T. Chuang and K. T. Nandakumar, *Chem. Eng. Res. Des., Trans. Inst. Chem. Eng.*, **76**, 843 (1998).
6. C. H. Fischer and J. L. Quarini, *AIChE meeting*, Miami Beach, FL (1998).
7. K. T. Yu, X. G. Yuan, X. Y. You and C. T. Liu, *Chem. Eng. Res. Des.*, **77a**, 554 (1999).
8. C. J. Liu, X. G. Yuan, K. T. Yu and X. J. Zhu, *Chem. Eng. Sci.*, **55**, 2287 (2000).
9. R. Krishna, J. M. van Baten, J. Ellenberger, A. P Higler and R. Taylor, *Chem. Eng. Res. Des., Trans. Inst. Chem. Eng.*, **77**, 639 (1999).
10. J. M. Van Baten and R. Krishna, *Chem. Eng. J.*, **77**, 143 (2000).
11. G. K. Gesit, K. Nandakumar and K. T. Chuang, *AIChE J.*, **49**, 910 (2003).
12. R. Rahimi, M. R. Rahimi, F. Shahraki and M. Zivdar, *Chem. Eng. Tech.*, **29**, 3 (2006).
13. R. Rahimi, M. R. Rahimi, F. Shahraki and M. Zivdar, *Distillation and Absorption IChemE Symposium*, **152**, 220 (2006).
14. X. L. Wang, C. J. Liu, X. G. Yuan and K. T. Yu, *Ind. Eng. Chem. Res.*, **43**, 255 (2004).
15. V. V. Ranade, *Academic press*, New York (2002).
16. R. Taylor, *Ind. Eng. Chem. Res.*, **46**, 4349 (2007).
17. M. Rahimi and M. Mohseni, *Korean J. Chem. Eng.*, **25**, 395 (2008).
18. R. Taylor and R. Krishna, John Wiley, New York (1993).
19. D. L. Bennett, Agrawal and P. J.Cook, *AIChE J.*, **29**, 434 (1983).
20. E. Nutter, US Patents, 5360583 (1994).
21. H. Z. Kister, McGraw-Hill, New York (1992).
22. M. J. Lockett, Cambridge University Press, Cambridge (1986).